COBEM 2021 26th International Congress of Mechanical Engineering
November 22-26, 2021, Virtual Congress, Brazil
ABCM Associação Brasileira de Engenharia e Ciências Mecânicas

COB-2021-2033
PARAMETER IDENTIFICATION BY UPDATING THE FINITE ELEMENT MODEL FOR A FLEXIBLE WING

Thiago Rosado de Paula
Vitor Paixão Fernandes
David Fernando Castillo Zuñiga
Alain Giacobini Souza
Roberto Gil Annes da Silva
Luiz Carlos Sandoval Góes
Instituto Tecnológico de Aeronáutica, São José dos Campos-SP 12228-900, Brasil
thiagorp@ita.br
vitor.paixao@ga.ita.br
davidfer@ita.br
giacobin@ita.br
gil@ita.br
goes@ita.br

Abstract. *There are several approaches for updating models to later model the aeroelastic behavior, and in this work Modal Assurance Criterion (MAC) was used to help estimate the parameters. The objective of this work was to update the finite element model for the EOLO aircraft wing. The Ground Test Vibration (GVT) modal formals were used as a comparison for the MAC, in addition to using the Nastran software to optimize the EOLO aircraft wing. It was found that the natural frequencies of the updated model approached the GVT data and the cross-correlation improved, but the correlation was far from ideal. It was concluded that the model was updated and improved compared to the initial model.*

Keywords: *MAC, GVT, Structural model, Natural frequencies, aeroelastic systems.*

1. INTRODUCTION

Currently, the study of flexible aircraft flight mechanics depends on the development of an aerodynamic model together with a structural model. The mechanical flight described not-linearly can be derived based on finite element models and aerodynamic theory, for example, lift surface theory, Vortex-Lattice Method (VLM) Doublet-Lattice Method, among others. However, accurate flight mechanics prediction is highly dependent on the accuracy of these structural models and aerodynamic (Gupta *et al.* (2015)).

The area of system identification is the area in which researchers turn their attention to the development of modeling methods inspired by experimental data acquisition to reduce the inaccuracy of the problem's analytical model. The model must be identified parametrically or non-parametrically. For the parametric identification of dynamic structures, the experimental modal analysis must be considered as a special area of the system identification for determining the modal analysis data (Mottershead and Friswell (1993)).

In the literature, it is common to find several methods to increase the accuracy of analytical/numerical structural models in relation to experimental data, updating the model parameters. (Gupta *et al.* (2015)). There are several approaches to updating models, as, for example, the Modal Assurance Criterion (MAC) which uses data from the modes shapes of the Ground Vibration Test (GVT) in relation to the modes shapes of the analytical/numerical models.

The objective of this work was to update the finite element model for the EOLO aircraft wing, identifying the Young's modulus and the specific mass using MAC to assess whether the estimated parameters have been improved.

2. FORM FUNCTIONS ARISING FROM GVT

To obtain the GVT data, Equations 1, 2 and 3 were used, in which are presented the modes shapes for the first three bending modes, the first symmetrical bending mode, the first antisymmetrical bending mode and the second symmetrical bending mode, considering the center of the string (Castillo Zuñiga *et al.* (2018)).For the second symmetrical mode, was selected the displacement of the left and right semi-spans and reflected to the opposite side. Then, an average between the displacements was performed. This was done to compensate for the antissymetry of the displacements obtained from the GVT and to make a better comparison between the GVT and the finite element model possible. Furthermore, in Figures

1a, 1b and 1c the behavior of the modes are presented in the wing simplification for a beam.

$$\phi_1 = 19,5539(0,00107088y^4 - 0,0302696y^2 + 0,00753852) \tag{1}$$

$$\phi_2 = -0,000101 - 0,06971y - 0,006363y^2 + 0,03919y^3 + 0,001514y^4 - 0,001882y^5 \tag{2}$$

$$\phi_3 = 0,005267 - 0,004512y + 0,01944y^2 + 0,006485y^3 - 0,01157y^4 - 0,0005317y^5 \tag{3}$$

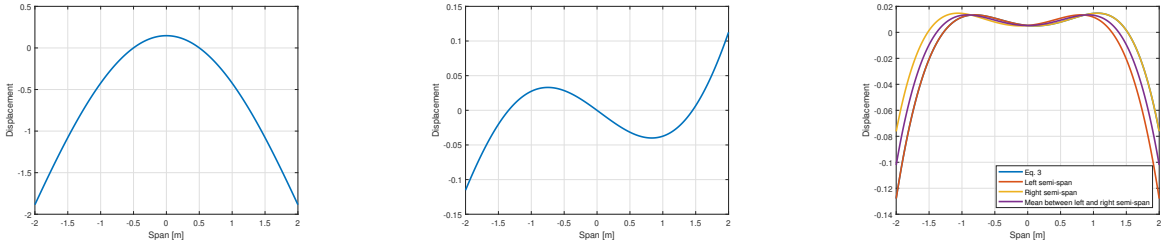

(a) Shape of the first symmetric bending mode from GVT (b) Shape of the first antisymmetric bending mode from GVT (c) Shape of the second symmetric bending mode from GVT

Figure 1: Behavior of the three first bending modes

3. MODAL ASSURANCE CRITERION

To assess the modes shape, the metric MAC was used, which is a standard metric in the literature (Gupta *et al.* (2015)), and measures the correlation between two different sources of data from the modes shapes for the same case. MAC is defined according to Equation 4.

$$MAC(\phi_{id,i}, \phi_{fe,i}) = \frac{|\phi_{id,i}^T \phi_{fe,i}|^2}{\phi_{id,i}^T \phi_{id,i} \phi_{fe,i}^T \phi_{fe,i}} \tag{4}$$

Where $\phi_{id,i}$ and $\phi_{fe,i}$ are the i-th modal vector of the GVT and FE model, respectively. The MAC value can range between 0 and 1, where 1 means the modal vectors are consistent.

4. FINITE ELEMENT OPTIMIZATION

In this work, the wing of the EOLO aircraft from the Aeronautical Systems Laboratory (LSA) of the Instituto Tecnológico de Aeronáutica (ITA) was used. The Figure 2 shows the model of the aircraft.

Figure 2: EOLO aircraft model.

For the simulations, the structural model of a beam was used to represent the structural model of the wing, as shown in Figure 3. Table 1 shows the basic configuration data for the simulations and the type of solution used.

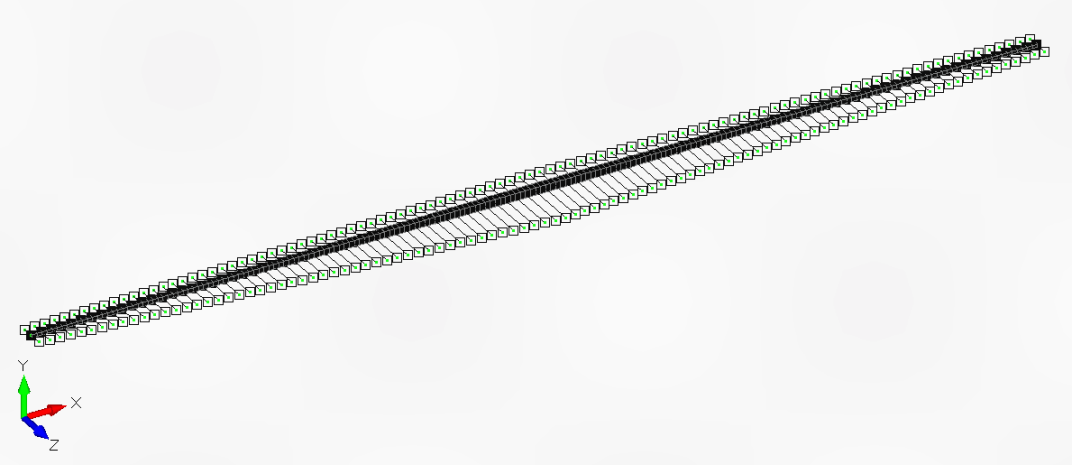

Figure 3: EOLO Wing Beam Model.

Table 1: Basic properties of the finite element model.

Nodes no.	201
Elements no.	200
Element type	Barra
Root section area (m^2)	8,6E-4
Tip section area (m^2)	2,3E-4
Aspect Ratio	19,00
Massa da asa (kg)	2,00

With this configuration, it is necessary to seek to bring the MAC value, between the two data sources, for each mode shape closer to 1, while reducing the difference between the modal frequencies of the GVT and those calculated through the finite element model (Gupta *et al.* (2015)). Thereby, it was used to Equation 5 to optimize the FEM (Zárate and Caicedo (2008)).

$$f = \sum_{i=1}^{n} \left[[1 - MAC(\phi_{id,i}, \phi_{fe,i})] + \left\| \frac{\omega_{id,i} - \omega_{fe,i}}{\omega_{id,i}} \right\| \right] \tag{5}$$

Which, n is the number of idenfied modes, $\omega_{id,i}$ e $\omega_{fe,i}$ are the i-th mode shape of the GVT and finite element model, repectively, and $\| \, \|$ $|| \, ||$ denote absolute value.

To optimize the Equation 5, Matlab was used to generate Nastran files and Genetic Algorithms to optimize the cost function. The nastran files ware run on MSC Nastran. Table 2 shows the configurations used for optimization. It is observed that the properties for Young's modulus and density were varied for each section. In addition, the initial value used for the optimization is verified. This initial value is the same used for the first simulation from the finite element method.

Table 2: Initial conditions and range of values for optimization.

	Young's modulu [Pa]			**Density** $[kg/m^3]$		
	Lower limit	**Initial**	**Upper limit**	**Lower limit**	**Initial**	**Upper limit**
Mat. 1	7.0E+10	7.2886E+12	9.0E+11	5.0E+01	9.6710E+01	1.5E+03
Mat. 2	4.0E+10	3.6445E+12	6.0E+11	5.0E+01	9.6710E+01	1.5E+03
Mat. 3	1.0E+10	3.3481E+08	6.0E+11	5.0E+01	9.6710E+01	1.5E+03
Mat. 4	1.0E+10	2.1971E+08	6.0E+11	5.0E+01	9.6710E+01	1.5E+03
Mat. 5	1.0E+10	1.9361E+08	6.0E+11	5.0E+01	9.6710E+01	1.5E+03
Mat. 6	1.0E+10	1.7729E+08	6.0E+11	5.0E+01	9.6710E+01	1.5E+03
Mat. 7	1.0E+10	1.4683E+08	6.0E+11	5.0E+01	9.6710E+01	1.5E+03
Mat. 8	1.0E+10	1.3748E+08	6.0E+11	5.0E+01	9.6710E+01	1.5E+03
Mat. 9	1.0E+10	1.2877E+08	6.0E+11	5.0E+01	9.6710E+01	1.5E+03
Mat. 10	8.0E+09	9.4432E+07	6.0E+11	5.0E+01	9.6710E+01	1.5E+03

5. RESULTS

5.1 Optimization

After the simulations, we arrived at Tables 3 and 4 resulting from the optimization. Table 3 demonstrates that the frequencies after optimization approached the GVT frequencies (Castillo Zuñiga *et al.* (2018)). After the optimization, the final values for the Young's modulus and the Density for each wing section were arrived at, as shown in Table 4.

Table 3: Natural frequencies for each mode.

	FEM (Hz)	**Updated FEM (Hz)**	**GVT (Hz)**
First symmetric	3.4850	7.0997	7.1000
First antisymmetric	5.5556	12.3288	13.7000
Second simétrico	12.5295	25.8083	22.1000

Table 4: Initial and final value for each wing property.

Young's Mod. [Pa]	**Initial value**	**Final value**	**Dens. $[kg/m^3]$**	**Initial value**	**Final Value**
E1	7.2886E+12	9.4870E+10	D1	9.6710E+01	1.2720E+03
E2	3.6445E+12	4.4599E+10	D2	9.6710E+01	1.2720E+03
E3	3.3481E+08	1.3080E+10	D3	9.6710E+01	1.2720E+03
E4	2.1971E+08	1.2292E+10	D4	9.6710E+01	1.2720E+03
E5	1.9361E+08	1.2089E+10	D5	9.6710E+01	1.2720E+03
E6	1.7729E+08	1.2062E+10	D6	9.6710E+01	1.2720E+03
E7	1.4683E+08	1.0377E+10	D7	9.6710E+01	1.2720E+03
E8	1.3748E+08	1.0365E+10	D8	9.6710E+01	1.2720E+03
E9	1.2877E+08	1.0170E+10	D9	9.6710E+01	1.2720E+03
E10	9.4432E+07	8.1918E+09	D10	9.6710E+01	1.2720E+03

5.2 Mode shapes

In Figures 4a, 5a and 6a the first three mode shapes of the aircraft wing are presented according to the acquired form function of the initial finite element model, the updated finite element model and the GVT. Figures 4a, 5a and 6a represent, respectively, the first symmetrical bending mode, the first antisymmetrical bending mode and the second symmetrical bending mode. Figures 4b, 5b and 6b represent the first three mode shapes of the aircraft wing from the updated finite element model.

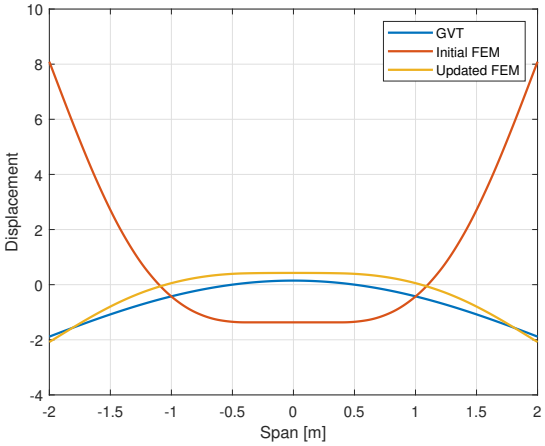

(a) First symmetric bending mode.

(b) First antisymmetric bending mode.

Figure 4: Behavior of the three first bending modes after optimization.

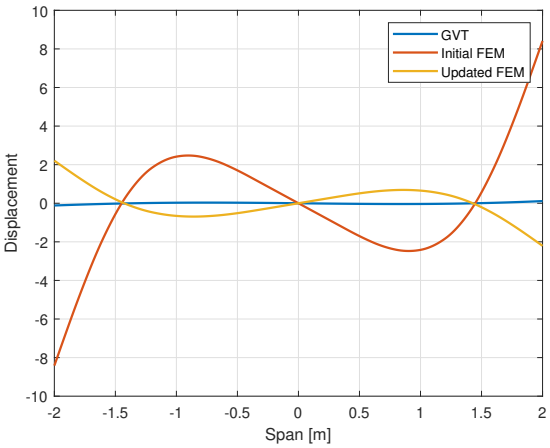

(a) First symmetric bending mode.

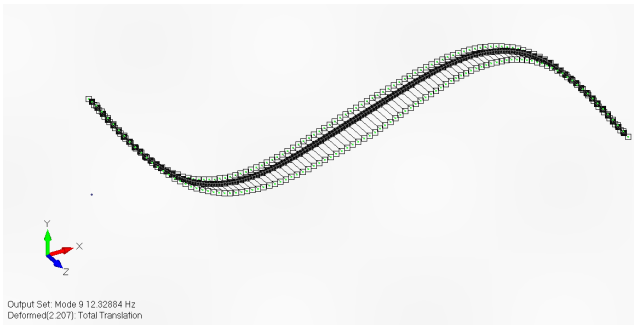

(b) First antisymmetric bending mode.

Figure 5: Behavior of the three first bending modes after optimization.

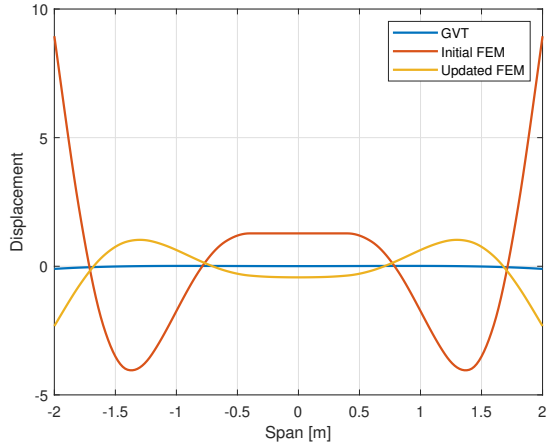

(a) First symmetric bending mode.

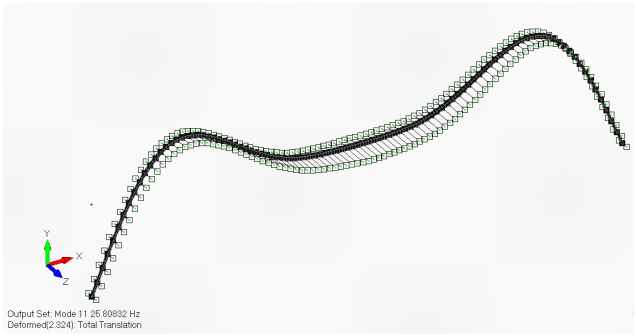

(b) First antisymmetric bending mode.

Figure 6: Behavior of the three first bending modes after optimization.

It is possible to observe that there was an approximation of the displacement values of the updated FEM in relation to the GVT in all studied modes compared to the initial FEM. However, as show in Figures 4a, 5a and 6a, the approach after the update was still not enough.

5.3 Modal Assurance Criterion results

Using Equation 4, it was found cross-correlation values between the initial FEM and updated FEM shown in Table 5 and Figure 7.

Table 5: MAC initial FEM and Updated FEM.

		Initial FEM		
	Mode\Mode	**First symmetric**	**First antisymmetric**	**Second symmetric**
Updated FEM	**First symmetric**	0.9955	0	0.0507
	First antisymmetric	0	0.9976	0
	Second symmetric	0.1351	0	0.9722

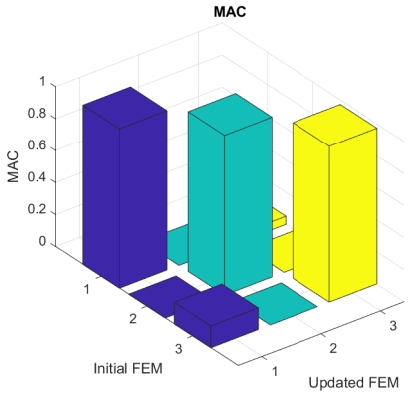

Figure 7: MAC initial FEM and Updated FEM.

It was verified on the MAC main diagonal that the autocorrelation is close to one, that is, the updated FEM has a high cross-correlation with the initial FEM. This demonstrates, together with Figures 4a, 5a and 6a, that the vertical displacements by the span for both the updated FEM and the initial FEM have similar values.

Similar to what was seen above, the values of the cross-correlation between the initial FEM and the GVT were found in Table 6 and Figure 8.

Table 6: MAC initial FEM and GVT.

		Initial FEM		
	Mode\Mode	**First symmetric**	**First antisymmetric**	**Second symmetric**
GVT	**First symmetric**	0.8061	0	0.0048
	First antisymmetric	0.0028	0.9772	0.0017
	Second symmetric	0.8772	0	0.3535

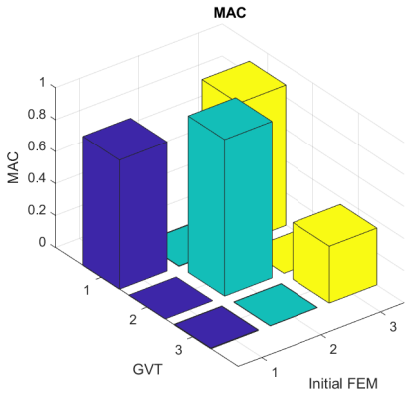

Figure 8: MAC initial FEM and GVT.

One can see on the main diagonal of the autocorrelation MAC that is close to a second end of the main diagonal, and an approximate value of 0.8 in the first term, but a value less than 0.4 in the third term of the main diagonal and, in addition, has a term outside the main diagonal with a correlation close to 0.87, that is, the initial FEM does not have a high cross-correlation with the GVT. This demonstrates, together with Figures 4a, 5a and 6a, that the vertical displacements by the span for the initial FEM are different from the GVT values.

Related to what was seen above, the cross-correlation values between the updated FEM and the GVT were shown in Table 7 and Figure 9.

Table 7: MAC updated FEM and GVT.

		Updated FEM		
	Mode\Mode	**First symmetric**	**First antisymmetric**	**Second symmetric**
GVT	**First symmetric**	0.8300	0	0.0178
	First antisymmetric	0.0033	0.9846	0.0014
	Second symmetric	0.8317	0	0.4402

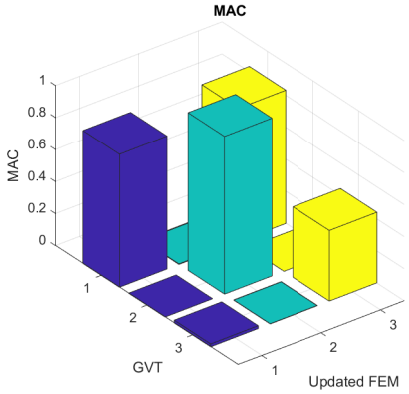

Figure 9: MAC updated FEM and GVT.

One can see on the main diagonal of the autocorrelation MAC that is close to a second end of the main diagonal and a value greater or equal than 0.8 in the first term, but an approximate value of 0.44 in the third term of the main diagonal and, in addition, it has a term off the main diagonal with a correlation close to 0.83, that is, the updated FEM does not have a high cross-correlation with the GVT. But, it appears that after updating the elements of the main diagonal and the term outside the main diagonal improved in relation to what was seen for the cross-correlation of the initial FEM and the GVT. This shows, together with Figures 4a, 5a and 6a, that the vertical offsets by span for the updated FEM are different from the GVT values, but are better than the initial FEM relative to the GVT.

In a similar way to what was seen above, the values of the GVT autocorrelation were shown in Table 8 and Figure 10.

Table 8: GVT autocorrelation for the first bending modes.

		GVT		
	Mode\Mode	**First symmetric**	**First antisymmetric**	**Second symmetric**
GVT	**First symmetric**	1	0.0078	0.5628
	First antisymmetric	0.0078	1	0.0006
	Second symmetric	0.5628	0.0006	1

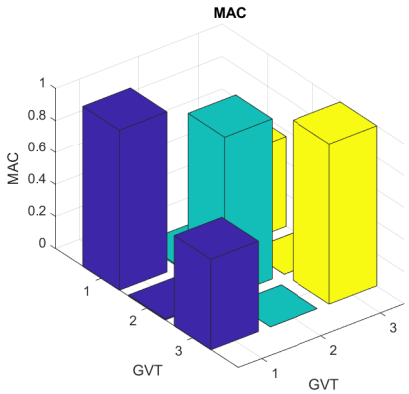

Figure 10: GVT autocorrelation for the first bending modes.

In Table 8 and Figure 10, there are two values on the secondary diagonal with values greater than 0.5, which demonstrates that the second symmetric bending mode is not entirely pure.

Figure 11 shows the complete autocorrelation for the GVT data (Castillo Zuñiga *et al.* (2018)). It is observed, comparing Figures 10 and 11, that for the second term in the dark blue column, in Figure 10 this value is close to zero while in Figure 10 it is a small value, but it is different from zero. It helps to understand that Equations 1, 2 and 3 still need to be improved.

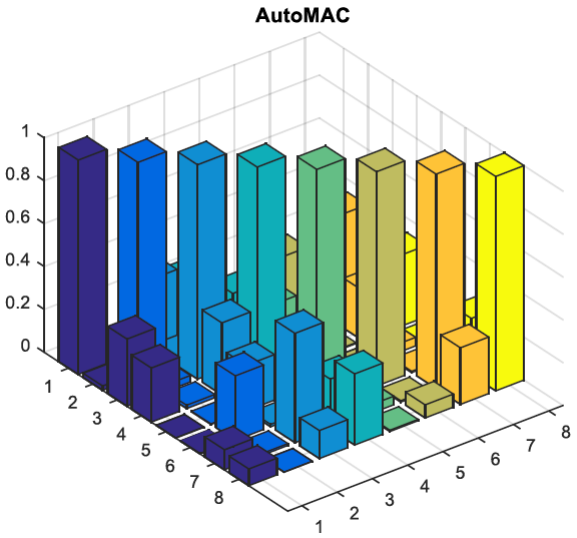

Figure 11: Autocorrelation with all EOLO wing modes. Castillo Zuñiga *et al.* (2018)

6. CONCLUSION

After optimization, the frequencies of each mode approximated to the GVT data for the wing.

But it was noticed that the MAC of the original simulation in FEM and the optimization obtained a correlation on the main diagonal close to 1.

Consequently, neither the FEM or the cross-optimized FEM correlation with the GVT are greater than 0.8 in all terms of the main diagonal. Furthermore, the FEM Optimized has a better behavior.

A small part of the error comes from the form functions, because comparing the data presented by Castillo Zuñiga *et al.* (2018) and the GVT auto-correlation through the form function provided, a small error is noticed.

Therefore, aiming to improve the update, it is necessary to use a wider range of values for material properties and improve the mode shape for each mode.

7. REFERENCES

Castillo Zuñiga, D.F., Sandoval, L.C., Barbosa, R., Maciel, B. and Drago, I., 2018. "Modal Testing of a Flexible Wing UAV". COBEM 2017, Curitiba, PR, Brazil, 2015. doi:10.26678/abcm.cobem2017.cob17-2477.

Gupta, A., Moreno, C.P., Pfifer, H. and Balas, G.J., 2015. "Updating a finite element based structural model of a small flexible aircraft". In *AIAA Modeling and Simulation Technologies Conference, 2015*. AIAA SciTech Forum, January. ISBN 9781624103438. doi:10.2514/6.2015-0903.

Mottershead, J.E. and Friswell, M.I., 1993. "Model updating in structural dynamics: A survey". *Journal of Sound and Vibration*, Vol. 167, No. 2, pp. 347–375. ISSN 0022460X. doi:10.1006/jsvi.1993.1340.

Zárate, B.A. and Caicedo, J.M., 2008. "Finite element model updating: Multiple alternatives". *Engineering Structures*, Vol. 30. ISSN 01410296. doi:10.1016/j.engstruct.2008.06.012.